Open access • Posted Content • DOI:10.1101/2021.09.29.462440

Loss of the cleaved-protamine 2 domain leads to incomplete histone-to-protamine exchange and infertility in mice — Source link

Lena Arévalo, Merges Ge, Simon Schneider, Oben Fe ...+2 more authors

Institutions: University Hospital Bonn

Published on: 01 Oct 2021 - bioRxiv (Cold Spring Harbor Laboratory)

Topics: Chromatin, Protamine, Prophase, Histone and DNA fragmentation

Loss of the cleaved-protamine 2 domain leads to incomplete histone-to-protamine exchange and infertility in mice

Lena Arévalo[1], Gina Esther Merges[1], Simon Schneider[1], Franka Enow Oben[1], Isabelle Neumann[1], Hubert Schorle[1]

[1] Department of Developmental Pathology, Institute of Pathology, University Hospital Bonn, Germany

Corresponding author: lena.arevalo@ukbonn.de, schorle@uni-bonn.de

Keywords: Protamines, PRM2 processing, chromatin, chromatin condensation, sperm, spermiogenesis, histone retention, protamine ratio

Abstract

Protamines are unique sperm-specific proteins that package and protect paternal chromatin until fertilization. A subset of mammalian species expresses two protamines (PRM1 and PRM2), while in others PRM1 is sufficient for sperm chromatin packaging. Alterations of the species-specific ratio between PRM1 and PRM2 are associated with infertility. Unlike PRM1, PRM2 is generated as a precursor protein consisting of a highly conserved N-terminal domain, termed cleaved PRM2 (cP2), which is consecutively trimmed off during chromatin condensation. The carboxyterminal part, called mature PRM2 (mP2), interacts with DNA and together with PRM1, mediates chromatin-hypercondensation. The removal of the cP2 domain is believed to be imperative for proper chromatin condensation, yet, the role of cP2 is not yet understood. We generated mice lacking the cP2 domain while the mP2 is still expressed. We show that the cP2 domain is indispensable for complete sperm chromatin protamination and male mouse fertility. cP2 deficient sperm show incomplete PRM2 incorporation, resulting in a severely altered protamine ratio, retention of transition proteins and aberrant retention of the testis specific histone variant H2A.L.2. During epididymal

transit, cP2 deficient sperm seem to undergo ROS mediated degradation leading to complete DNA fragmentation. The cP2 domain therefore seems to be a key aspect in the complex crosstalk between histones, transition proteins and protamines during sperm chromatin condensation. Overall, we present the first step towards understanding the role of the cP2 domain in paternal chromatin packaging and open up avenues for further research.

Introduction

Chromatin structure and dynamics in the sperm nucleus are as unique as the sperm cell itself, and are of major importance to sperm function, fertilizing ability, and embryo survival. Paternal DNA is particularly vulnerable to damage, especially to oxidative stress during epididymal sperm maturation and migration, leading to a higher requirement for protection (Chen et al. 2002). At the same time, the size and shape of the sperm cell nucleus needs to be optimized for efficient sperm movement through the female reproductive tract (Tourmente et al. 2011). This is achieved by the complete reorganization of paternal chromatin from nucleo-histone to nucleo-protamine during the final steps of spermatogenesis (Balhorn 2007, Rathke et al. 2014).

Even though many studies have demonstrated that the correct execution of this transition is imperative for male fertility and embryo survival (Aoki and Carrell 2003), surprisingly little is known about the process itself. Recent studies have only just started to unravel its molecular basis (Schneider et al. 2016, Barral et al. 2017, Hada et al. 2017). Barral et al. (2017) were able to show that the testis specific histone variant H2A.L.2 together with TH2B and transition proteins (TNP1 and TNP2) mediates structural changes in chromatin allowing protamines to bind DNA. Protamines are small, arginine-rich proteins. Their high arginine content allows them to bind DNA with high affinity and to shield the charges of the DNA backbone more efficiently than histones (Balhorn 1989, Tanaka and Baba 2005). Two types of protamines have been identified in mammals: protamine 1 (*PRM1*, PRM1) and protamine 2 (*PRM2*, PRM2). While PRM1 is a major sperm protamine found across mammals, PRM2 is only detected in the sperm of primates, most rodents, and a subset of other placental

mammals (Chauviere et al. 1992, Retief and Dixson 1993). The coding regions of *PRM1* and *PRM2* are tightly clustered and map to a small section of chromosome 16. It is highly likely that *PRM2* is the result of a *PRM1* duplication event (Krawetz and Dixon 1988, Lüke et al. 2011).

Unlike PRM1, PRM2 is transcribed as a precursor. The N-terminal region of the translated PRM2, termed cleaved-PRM2 (cP2), is successively cleaved over several days while chromatin condensation is taking place. After this, only mature-PRM2 (mP2) remains bound to the completely condensed DNA (Retief et al. 1993, Balhorn 2007, Yelick et al. 1987, Oliva and Dixon 1991). Perturbations of PRM2 processing has been shown to lead to decreased DNA integrity and sperm dysfunction (deYebra et al. 1998, Torregrosa et al. 2006). In previous comparative evolutionary studies, it was shown that the cP2 coding sequence is conserved in both primates and rodents. mP2, however, evolves under less selective constraint (Lüke et al. 2011, 2016). Changes in coding sequences of cP2 were associated with differences in sperm head size in mouse species. This association was specific to the cP2 domain and not found for mP2 (Lüke et al. 2014a). A potential reason for this pattern is that changes in cP2 are selected against conserving a crucial function for reproduction, while mP2 is free to evolve under less constraint due to its proposed functional redundancy to PRM1 (Lüke et al. 2011, 2016).

Proper PRM2 cleaving therefore seems to be crucial for successful reproduction, yet, the function of the cP2 domain and PRM2 processing are unknown to date. Establishment and analysis of PRM2 deficient mice revealed that $Prm2^{-/-}$ males were infertile, while $Prm2^{+/-}$ males remained fertile (Schneider et al. 2016). Of note, mice deficient for TNP1, TNP2 and H2A.L.2 show incomplete PRM2 processing (PRM2 precursor detected in mature sperm nuclei) (Yu et al. 2000, Zhao et al. 2001, 2004, Barral et al. 2017).

Given that cP2 cleaving is taking place during DNA condensation in late spermiogenesis, the strong evolutionary conservation of this domain and the effect of incomplete PRM2 processing on sperm function and fertility, cP2 is likely to play an important role in the correct execution of chromatin condensation. We therefore studied the involvement of cP2 in

chromatin condensation during spermiogenesis by generating and analyzing a mouse line bearing a deletion of cP2, while maintaining mP2 expression. We analyzed fertility, testis and sperm morphology, chromatin integrity and nuclear protein content of these mice and revealed that $Prm2^{\Delta c/+}$ mice are already infertile and that cP2 seems necessary for complete protamination of sperm chromatin.

Material and Methods

Animals

For the generation of mouse lines using CRISPR/Cas9 the F1 generation of mouse strains C57Bl6 and DBA2 (B6D2F1) were used. Founder animals were backcrossed to C57Bl6. Mice were maintained under standard laboratory conditions in environmentally controlled rooms (20–24ºC) on a 12L:12D photoperiod with nesting material and ad libitum food and water. All animal experiments were conducted according to German law of animal protection and in agreement with the approval of the local institutional animal care committees (Landesamt für Natur, Umwelt und Verbraucherschutz, North Rhine-Westphalia, Germany, AZ81-02.04.2018.A369).

Gene-edited mouse lines

Guide RNA (gRNA) sequence pre-selection was performed using the algorithm published by Hsu et al. (2013). Two gRNA sequences were selected based on quality scores in each case maximizing specificity and minimizing off-target action (score > 50) (Table S1). The designed guide sequences were ordered as crisprRNA sequences (crRNA) (IDT, Leuven, Belgium) and annealed to tracrRNA (IDT) by incubating 5min at 95°C for a final concentration of 50mM of gRNA (crRNA+tracrRNA). The target site of the designed gRNAs is shown in figure S1A. The repair template used for homology directed repair (HDR), here single-stranded oligodeoxynucleotides (ssODNs) (IDT) (Yoshimi et al. 2014, 2016), are shown in figure S1B. Ribonucleoprotein (RNP) complexes were assembled immediately prior to delivery by incubation of 4pmol/µl Cas9 (IDT) protein, 4pmol/µl of each gRNA and 10pmol/µl ssODN in

Opti-MEM medium (Thermo Fisher Scientific, Waltham, USA) for 10min at room temperature.

To generate gene-edited founder animals, B6D2F1 females were hormonally superovulated and mated as described (Schneider et al. 2016). Oocytes were isolated from the oviducts, washed and transferred into droplets of Opti-MEM medium containing the previously prepared RNP complex and electroporated using a BioRad Gene Pulser (BioRad, Feldkirchen, Germany) (two 3ms square wave pulses at 30V with an 100ms interval). Oocytes were recovered and washed 5x in M2 medium (Merck Millipore, Darmstadt, Germany) followed by 3 washes in KSOM (Merck Millipore) medium droplets. Oocytes were then incubated in KSOM medium covered in paraffin oil overnight at 37°C. Developing 2-cell stage embryos were then transferred into the oviducts of pseudo-pregnant foster mice. Offspring was genotyped (primers, see Fig. 1A, Table S1) and positive founder animals backcrossed to C57Bl/6J for at least 3 generations before analysis. Male mice between 10 and 13 weeks of age were used for analysis.

Fertility analysis

Five males per genotype were mated with C57Bl/6J females 1:2 and females were checked daily for the presence of a vaginal plug until at least 5 plugs per male were observed. Pregnancy rate and litter size were noted.

Sampling and mature sperm isolation

The testes were dissected and weighed. For paraffin sectioning, testes and epididymides were fixed in either Bouin's solution for histology or in 4% Paraformaldehyde solution for immunohistochemistry (IHC). For tubule preparations testes were transferred to PBS and tubules dissected as described in Kotaja et al. (2004). Briefly, tubules were separated and elongating and condensed spermatid containing sections were identified through their light absorption pattern using a dissection microscope. Tubule sections were squashed on a slide, frozen in liquid nitrogen for 20 seconds, fixed in 90% ethanol for 5 minutes and air dried.

Tubule preparations were used for IHC. To obtain sperm samples, caudae epididymes were dissected and transferred to preheated (36-37°C) M2 medium, incised several times, squeezed with tweezers several times during a 30min incubation period at 36-37°C to ensure flushing out the whole sperm population including immotile sperm.

Histology

Bouin-fixed testes and epididymes were paraffized, embedded in paraffin blocks and sectioned at 3 microns. Sections were deparaffinized and stained with the Periodic acid–Schiff (PAS) procedure. Stained sections were imaged under bright field at 20x and 63x magnification using a Leica DM5500 B microscope (Leica Microsystems, Wetzlar, Germany).

Basic sperm analysis

Isolated spermatozoa were counted for 6-12 animals per genotype using a hemocytometer. Sperm motility was analyzed for 3-4 animals per genotype by taking 5-10, 3 second video clips per animal using a Basler acA1920-155ucMED camera (Basler AG, Ahrensburg, Germany). A minimum of 200 sperm per individual were analyzed and the percentage of motile sperm calculated. Sperm viability was analyzed by eosin-nigrosin staining for 3-4 animals per genotype. Approximately 1 x 10^6 sperm were mixed with 50µl of eosin-nigrosin dye, incubated for 30 seconds, spread on slides, air-dried and cover-slipped. A minimum of 200 spermatozoa were analyzed under bright field (Leica DMIRB microscope) and the percentage of viable spermatozoa calculated.

RNAseq and differential expression analysis

RNA was extracted from testes after removal of the tunica albuginea using the RNeasy kit (Qiagen, Hilden, Germany). RNA integrity (RIN) was determined using the RNA Nano 6000 Assay Kit with the Agilent Bioanalyzer 2100 system (Agilent Technologies, Santa Clara, CA, USA). RIN values ranged from 7.3–10 for all samples. RNA sample quality control and library preparation were performed by the University of Bonn Core facility for Next Generation

Sequencing (NGS), using the QuantSeq 3'-mRNA Library Prep (Lexogen, Greenland, NH, USA). RNAseq was performed by the University of Bonn Core facility for Next Generation Sequencing (NGS) on the Illumina HiSeq 2500 V4 platform, producing >10 million, 50bp 3'-end reads per sample.

The samples were then mapped to the mouse genome (GRCm38.89) using HISAT2 2.1 (Kim et al. 2015). StringTie 1.3.3 (Pertea et al. 2015) was used for transcript quantification and annotation. Gene annotation was retrieved from the Ensembl FTP server (ftp://ftp.ensembl.org)(GRCm38.89). The python script (preDE.py) included in the StringTie package was used to prepare DEseq2-compatible gene-level count matrices for analysis of differential gene expression. Mapping to the *Prm2* genomic location was visualized using the Integrative Genomics Viewer (IGV; Robinson et al. 2011).

Differential expression (DE) was analyzed using DESeq2 1.16.1 (Love et al. 2014). The adjusted p-value (Benjamini-Hochberg method) cutoff for DE was set at < 0.05, log2 fold change of expression (LFC) cutoff was set at > 1. We performed GO term and pathway overrepresentation analyses on relevant lists of genes using the PANTHER gene list analysis tool with Fisher's exact test and FDR correction (Mi et al. 2017).

Sperm nuclear morphology

Nuclear morphology was analyzed for 3 individuals per genotype. Approximately 1.5×10^6 sperm were fixed in methanol-acetic acid (3:1), spread onto a slide and stained with 4′,6-diamidino-2-phenylindole (DAPI) nuclear stain (ROTI®Mount FluorCare DAPI (Carl Roth GmBH, Karlruhe, Germany)). At least 200 stained sperm cells per individual were imaged at 100x magnification using a Leica DM5500 B fluorescent microscope. Nuclear morphology was analyzed using the stand-alone version of the Nuclear Morphology program by Skinner et al. (2019). The program allows for automated detection and morphological analysis of mouse sperm nuclei (among other species and cell types). It additionally provides options for clustering heterogenous populations by nuclear parameters and comparative analyses of

196 nuclear morphology (Skinner et al. 2019). The parameters used for nucleus detection are
197 shown in figure S3.
198
199 Sperm basic nuclear protein extraction and analysis
200 Basic nuclear proteins were extracted described in Soler-Ventura et al. (2018). Briefly,
201 approximately 10 x 10^6 of swim-out sperm were washed in PBS and pelleted. The pellet was
202 resuspended in buffer containing 1M Tris pH 8, 0.5M MgCl and 5ul Triton X-100.
203 Subsequently the pellet was treated with 1mM PMSF in water inducing cell lysis. Treatment
204 with EDTA, DTT and GuHCl induced DNA denaturation. Incubation at 37°C for 30min in
205 presence of 0.8% vinylpyridine is necessary for mouse protamine separation on the
206 subsequent protein gel. DNA is then precipitated by addition of EtOH and separated from the
207 sample by centrifugation. Basic sperm nuclear proteins are then extracted and dissolved in
208 0.5M HCl, followed by protein precipitation with TCA, acetone washes and drying. The
209 precipitated proteins are resuspended in sample buffer containing 5.5 M urea, 20% β-
210 mercapto-ethanol and 5% acetic acid.
211 The samples were then run on a pre-electrophorized acid-urea polyacrylamide gel (AU-
212 PAGE) (2.5 M urea, 0.9 M acetic acid, and 15% acrylamide/0.1% N,N′-Methylene bis-
213 acrylamide, TEMED and APS). The extracted basic nuclear proteins migrate towards the
214 negative pole at a 150V for 1h, 50min. The gels were stained with Coomassie Brilliant Blue
215 (Sigma Aldrich, Taufkirchen, Germany) using standard procedures. The two main protamine
216 bands can be observed in the bottom of the gel with mature-PRM2 corresponding to the
217 upper and PRM1 the lower band (Ishibashi et al. 2010, Soler-Ventura et al. 2018). PRM2
218 precursor bands can be observed in the lower part of the gel above the mature-PRM2 band,
219 if present (Yu et al. 2000, de Mateo et al. 2011). In the upper half of the gel, bands
220 corresponding to other basic nuclear proteins, including histones can be found (see Soler-
221 Ventura 2018). The densities of Coomassie stained bands were analyzed using ImageJ
222 (1.52k, Schneider et al. 2012).
223

Immunohistochemistry

PFA fixed testis and epididymis sections as well as EtOH fixed tubule preparations were used for immunofluorescent staining. Sections were deparaffinized in xylol and rehydrated. Sections and tubule preparations were washed in PBS and blocked for 30 min with normal horse serum (Vectorlabs, Burlingame, USA) at room temperature, followed by primary antibody incubation over night at 4°C. Antibodies and dilutions are shown in table S3. Slides were then double-stained with fluorescent secondary antibodies using the VectaFluor™ Duet Immunofluorescence Double Labeling Kit, DyLight® 594 Anti-Rabbit (red), DyLight® 488 Anti-Mouse (green) (Vectorlabs, Burlingame, USA), DAPI counterstained and coverslipped with ProLong™ Gold antifade reagent with DAPI (Thermo Fisher Scientific, Waltham, USA).

Mass spectrometry and differential protein abundance analysis

Basic nuclear protein extractions were done for 3 individuals per genotype using approximately 10^6 sperm. Extracted proteins were dissolved in sample buffer (5.5 M urea, 20% β-mercapto-ethanol and 5% acetic acid).

Peptide preparation: Protein solutions (5.5 M urea, 20% 2-mercaptoethanol, 5% acetic acid) were dried in a vacuum concentrator and subjected to in solution preparation of peptides. Proteins were dissolved in 50 mM acrylamide solution (Tris-HCl, pH=8) and alkylated for 30 min at RT. 1 µg of Trypsin were added for o/n proteolysis at 37°C. Dried peptides were dissolved in 10 µL 0.1% trifluoro acetic acid (TFA) and desalted with ZipTips (Waters GmbH, Eschborn, Germany) according to standard solid-phase extraction procedures. Equilibration and binding was done in presence of 0.1% TFA, washing with 0.1% formic acid (FA). Eluates (50% acetonitrile, 0.1% FA) were dried and stored at -20°C.

LC-MS measurements: Peptide separation was performed on a Dionex Ultimate 3000 RSLC nano HPLC system (Dionex GmbH, Idstein, Germany). The autosampler was operated in µl-pickup mode. Peptides were dissolved in 10 µl 0.1% FA (solvent A). 2 µL were injected onto a C18 analytical column (300 mm length, 75 µm inner diameter, ReproSil-Pur 120 C18-AQ, 1.9 µm). Peptides were separated during a linear gradient from 2% to 35% solvent B (90%

acetonitrile, 0.1% FA) within 90 min at 300 nl/min. The nanoHPLC was coupled online to an Orbitrap Fusion Lumos mass spectrometer (Thermo Fisher Scientific, Bremen, Germany). Peptide ions between 300 and 1600 m/z were scanned in the Orbitrap detector every 3 seconds with R=120,000 (maximum fill time 50 ms, AGC target 400,000). Polysiloxane (445.12002 Da) was used for internal calibration (typical mass error ≤1.5 ppm). In a top-speed method peptides were subjected to higher energy collision induced dissociation (HCD: 1.0 Da isolation, threshold intensity 25,000, normalized energy 27%) and fragments analyzed in the Orbitrap with target 50,000 and maximum injection time 22 ms, R=15,000. Fragmented peptide ions were excluded from repeat analysis for 20 s.

Data analysis: Raw data processing and was performed with Proteome Discoverer software 2.5.0.400 (Thermo Fisher Scientific). Peptide identification was done with an in-house Mascot server version 2.6.1 (Matrix Science Ltd, London, UK). MS data were searched against *Mus musculus* sequences from SwissProt (2021/03, including isoforms), and contaminants (cRAP, Mellacheruvu et al. 2013). Precursor Ion m/z tolerance was 10 ppm, fragment ion tolerance 20 ppm. Tryptic peptides with up to two missed cleavages were searched. Propionamide on cysteines was set as static modification. Oxidation was allowed as dynamic modification of methionine, acetylation as modification of protein N-termini. Mascot results were evaluated by the percolator algorithm (Kall et al. 2008) version 3.05 as implemented in Proteome Discoverer. Spectra with identifications below 1% q-value were sent to a second round of database search with semitryptic enzyme specificity (one missed cleavage allowed). Protein N-terminal acetylation, methionine oxidation, carbamylation on lysine and N-termini were allowed as dynamic modifications. Actual FDR values were typically ≤0.5% (peptide spectrum matches), ≤1.0% (peptides), <1% (proteins). Proteins were accepted if at least two peptides with q-value <1% were identified. Summed abundances (areas of precursor extracted ion chromatograms of unique peptides) were used for relative quantification.

Differential abundance (DA) analysis: DA analysis was performed using the Bioconductor package proDA (Ahlmann-Eltze C 2021) using peptide spectrum matches (PSM) level data

extracted from Protein Discoverer. Only proteins detected in all genotypes and all replicates with more than two peptides were included in the analysis. The data were log2 transformed and median normalized prior to DA analysis to ensure comparability. The proDA package is based on linear models and utilized Bayesian priors to increase power for differential abundance detection (Ahlmann-Eltze C 2021). Proteins with a log2 fold change (LFC) of >1 and false discovery rate adjusted p-value (FDR) <0.05 were considered differentially abundant compared to the WT. Plots were generated using the R-package ggplot2 (Wickam 2016).

Generation of expression plasmids and transfection

Prm2 and Prm2$^{\Delta c}$ cDNA (GenBank: NM_008933.2) was amplified from C57Bl6 mouse testis cDNA using overhang primers introducing suitable restriction enzyme motifs (table S1) and cloned N-terminally in-frame with eGFP into the pEGFP-N3 vector (6080-1). Correct sequence and insertion were verified by sequencing.

Human Embryonic Kidney 293 (HEK293) cells were cultured in standard medium (DMEM, 10% FBS). HEK293 cells were transfected at 80% confluence with 3 µg of pPrm2-EGFP-N3 (*Prm2*), pPrm2$^{\Delta c}$-EGFP-N3 (Prm2$^{\Delta c}$ sequence) or pEGFP-N3 with FuGENE® HD Transfection Reagent (Promega, Madison, USA), according to the manufacturer's instructions. At 12 hours post-transfection the medium was changed. Pictures were taken after 48 hours using a Leica DMIRB inverted microscope (Leica Microsystems, Wetzlar, Germany).

Results

Generation of gene-edited mouse lines

To delete cP2 in the reading frame of the PRM2 gene, we used CRISPR/Cas9 with templates catalyzing homology directed repair (HDR). In order to induce the deletion, we used two gRNAs targeting the 5' and 3' ends of the cP2 domain (Fig. 1A, Fig. S1). A single stranded DNA template encoding the 5' and 3' areas flanking the cP2 coding region enabling

deletion of the cP2 coding region and an in-frame repair, generating an allele, where only mature PRM2 is expressed from the endogenous promoter, was added to the gene-editing reaction (Fig. S1). The sequence of the generated allele, named $Prm2^{\Delta c}$, is shown in figure S1A and was registered with the mouse genomics database (MGI:6718282). Animals were generated, sequence validated and backcrossed to C57Bl/6J for at least 3 generations before analysis.

$Prm2^{\Delta c/+}$ as well as $Prm2^{\Delta c/-}$ male mice are infertile

First, we subjected the $Prm2^{\Delta c/+}$ mice to a fertility test. Five $Prm2^{\Delta c/+}$ male mice were mated to ten WT females and the pregnancy/litters were recorded for five confirmed vaginal plugs per male (successful matings). We found that $Prm2^{\Delta c/+}$ male mice were infertile, with no observed pregnancies in at least five confirmed matings each. This is in contrast to the deletion of the entire PRM2 gene, where $Prm2^{+/-}$ male mice remained fertile (Schneider et al. 2016) (Fig. 1B). We hypothesized that an aberrant interaction between the newly generated mP2 and the PRM2 precursor expressed from the wildtype allele might lead to interference and be causative for infertility in these males. In order to test this, we bred $Prm2^{\Delta c/+}$ females with $Prm2^{+/-}$ males published by us ($Prm2^{\Delta 97bp}$; Schneider et al. 2016, MGI:5760133) to generate $Prm2^{\Delta c/-}$ mice. This results in male mice, in which only $Prm2^{\Delta c}$ is present and expressed. However, $Prm2^{\Delta c/-}$ males did not produce any litters in at least five confirmed matings each and can be considered infertile (Fig. 1B). This strongly suggests, that the cP2 domain is essential for murine spermiogenesis. If cP2 was non-essential these $Prm2^{\Delta c/-}$ mice should be fertile, similar to $Prm2^{+/-}$ males.

mP2 is expressed in $Prm2^{\Delta c/-}$ mice and transcriptional silencing does not seem to be disrupted

Since the $Prm2^{\Delta c/-}$ mice allow for detection and validation of mP2 transcripts from the $Prm2^{\Delta c}$ allele we, performed RNAseq on testis samples and analyzed expression of *Prm2*. By mapping the RNAseq reads to the *Prm2* genomic location, we were able to verify that the

mP2 transcript was indeed expressed from the gene edited Prm2$^{\Delta c}$ allele (Fig. S2). The expression levels of the *Prm2* transcripts were comparable in all genotypes (WT, Prm2$^{\Delta c/+}$ and Prm2$^{\Delta c/-}$), thus the alleles do not display a gene dosage effect (Fig. 1C).

In our previous study we found that in the Prm2$^{-/-}$ testis, a much higher number of genes was differentially higher than lower expressed (81:13) indicating incomplete protamine-mediated transcriptional silencing (Schneider et al. 2020). Here, compared to WT, we found 36 genes differentially higher expressed and 42 genes differentially lower expressed for Prm2$^{\Delta c/+}$ males and 26 genes differentially higher and 43 differentially lower for Prm2$^{\Delta c/-}$ (Fig. 1D). This indicates that transcriptional silencing is not notably disrupted in males harboring the Prm2$^{\Delta c}$ allele. No GO-term or pathway enrichment was found for analyzed gene sets. Lists of differentially expressed genes and statistics can be found in supplementary dataset S1.

mP2 is detected in Prm2$^{\Delta c/+}$ and Prm2$^{\Delta c/-}$ spermatid nuclei, but is also found in cytoplasm and residual bodies

After confirming, that the gene-edited mP2-domain is expressed from the Prm2$^{\Delta c}$ allele, we next addressed the question, whether mP2 can be detected in spermatids and is able to condense DNA. We therefore first performed IHC on PFA fixed testis sections. The epitope of the PRM2 antibody (Hup2B, Briarpatch Bio, Livermore, USA) is located in the first half of the mP2 domain and is able to detect both, the PRM2 protein generated from the wildtype and the gene-edited Prm2$^{\Delta c}$ allele. As shown in figure 2A, PRM2 is detected in condensed spermatid nuclei of Prm2$^{\Delta c/+}$ and Prm2$^{\Delta c/-}$ males, similar to the wildtype. However, we additionally detected a signal in the cytoplasm of spermatids and residual bodies that is strongest in Prm2$^{\Delta c/-}$ males and not found in wildtype (Fig. 2A).

To determine if mP2 is able to condense DNA, we expressed PRM2 and the mP2 sequence of the Prm2$^{\Delta c}$ allele tagged with eGFP in HEK293 cells. The ability of PRM1 to bind to DNA and condense nuclei when expressed *in vitro* in somatic cells had been demonstrated before by Iuso et al. (2015) in sheep fibroblasts. Experiments revealed that PRM2-eGFP and

363 Prm2$^{\Delta c}$-eGFP locate to the HEK293 cell nuclei and are present after 48h as large speckles in
364 the nucleus (Fig. 2B). We therefore concluded that mP2 is able to condense the nucleus of
365 somatic cells *in vitro* and should therefore be able to contribute to spermatid chromatin
366 condensation *in vivo*.
367
368 Testis histology is inconspicuous, while mature sperm are inviable and immotile in Prm2$^{\Delta c/+}$
369 and Prm2$^{\Delta c/-}$ male mice
370 Next, we analyzed testis mass and examined histological sections to determine the nature of
371 the infertility. Relative testes mass did not differ from the wildtype (Fig. 3A). Almost no viable
372 and motile mature sperm were found in Prm2$^{\Delta c/+}$ and Prm2$^{\Delta c/-}$ males (Mean percent viable:
373 Prm2$^{\Delta c/+}$=1.7, SD=1.31; Prm2$^{\Delta c/-}$=0; Mean percent motile: Prm2$^{\Delta c/+}$=0.2, SD=0.45; Prm2$^{\Delta c/-}$
374 =0.25, SD=0.5) (Fig. 3A, Fig. S4). Interestingly, sperm count is significantly reduced in
375 Prm2$^{\Delta c/-}$ but not in Prm2$^{\Delta c/+}$ males compared to the wildtype (ANOVA: $F(2)=10.87$, $p<0.001$;
376 Post-hoc Tukey HSD: WT vs. Prm2$^{\Delta c/+}$: $p=0.89$, WT vs. Prm2$^{\Delta c/-}$: $p<0.001$) (Fig. 3A). To
377 determine if the loss of cP2 affects spermiogenesis, testis and epididymis histology was
378 evaluated by PAS staining of Bouin-fixed sections. Testis histology was inconspicuous and
379 spermatogenesis seemed not to be affected in either genotype (Fig. 3B). Epididymis
380 histology however, shows larger round cells and vacuole-like structures, which are indicative
381 of spermatid degradation. This was more pronounced in Prm2$^{\Delta c/-}$ males compared to Prm2$^{\Delta c/+}$
382 males (Fig. 3B).
383
384 Chromatin integrity is strongly affected and nuclear morphology is altered in Prm2$^{\Delta c/+}$ and
385 Prm2$^{\Delta c/-}$ male mice.
386 Since protamines condense sperm chromatin and were shown to influence sperm head
387 morphology (Lüke et al. 2014a,b), mature sperm DNA integrity and nuclear morphology
388 could be affected even though mP2 is able to condense DNA. We therefore extracted DNA
389 from mature sperm and subjected it to agarose gel electrophoresis. DNA from sperm of
390 Prm2$^{\Delta c/+}$ males is completely fragmented (Fig. 4A). Schneider et al. (2020) was able to show

that during epididymal transit, $Prm2^{-/-}$ deficient sperm underwent ROS mediated destruction, leading to DNA and membrane degradation and immotility. We therefore stained sections of epididymides against 8-Oxo-2'-deoxyguanosine (8-OHdG), which indicates oxidative DNA damage. In the caput epididymis we detected only a slight increase of the 8-OHdG signal in $Prm2^{\Delta c/+}$ and $Prm2^{\Delta c/-}$ males compared to the wildtype. However, in the $Prm2^{\Delta c/+}$cauda epididymis a strong increase in 8-OHdG was visible compared to the wildtype. The 8-OHdG signal in the $Prm2^{\Delta c/-}$ cauda was less intense, which is likely due to the more severe degradation and reduced sperm count (Fig. 4B).

Nuclear morphology analysis revealed aberrant nuclear morphology of mature sperm in $Prm2^{\Delta c/+}$ and $Prm2^{\Delta c/-}$ males. Sperm from both genotypes show a significantly reduced nuclear size compared to the WT (Table S2, Fig. 4C, Fig. S5). $Prm2^{\Delta c/+}$ males show two clusters of nuclear shape, a slimmer nucleus with decreased hook curvature and a smaller hookless nucleus. This phenotype is even more severe in $Prm2^{\Delta c/-}$ males (Table S2, Fig. 4C, Fig. S5). Of note, nuclear morphology of $Prm2^{\Delta c/-}$ and $Prm2^{\Delta c/+}$ deficient sperm also differs from $Prm2^{+/-}$ and $Prm2^{-/-}$ males.

<u>The protamine ratio is flipped in $Prm2^{\Delta c/+}$ and $Prm2^{\Delta c/-}$ males</u>

Since the ratio between PRM1 and PRM2 is constant in mature sperm (in mice ~60% PRM2), and alterations of this ratio are associated with sperm defects and infertility (Corzett et al. 2002, Steger et al. 2008; García-Peiró et al. 2011), we next tested if male mice harbouring the $Prm2^{\Delta c}$ allele display alterations of the PRM1/PRM2 ratio. Interestingly, acid-urea gel electrophoresis (AU-PAGE) of mature sperm basic nuclear proteins showed several bands corresponding to PRM2 precursors in $Prm2^{\Delta c/+}$ males. This was also the case in $Prm2^{+/-}$ males.

Comparing the densities of the PRM1 band relative to mP2 and PRM2 precursor bands, we found the PRM ratio to be strongly altered, showing a lower percentage of PRM2 (including precursors) compared to the wildtype in $Prm2^{\Delta c/+}$ and $Prm2^{\Delta c/-}$ males (Mean %PRM2: WT=69,29; $Prm2^{\Delta c/+}$=42,07; $Prm2^{\Delta c/-}$=26.78)(ANOVA: F(2)=18.98,p=0.009; Post-hoc Tukey

HSD: WT vs. $Prm2^{\Delta c/+}$: p=0.04, WT vs. $Prm2^{\Delta c/-}$: p=0.008). This does not seem to be the case in $Prm2^{+/-}$ males, for which we find the percentage of PRM2 (including precursors) to be similar to the wildtype (%PRM2=66.57 (n=1)) (Fig. 4D, Fig. S7). These data, together with the mP2 signal detected in condensing spermatid cytoplasm (Fig. 2A), strongly suggest, that loss of the cP2 domain leads to a reduction of PRM2 associated with DNA.

Histone-to-protamine transition is incomplete in $Prm2^{\Delta c/+}$ and $Prm2^{\Delta c/-}$ males

Since we found the relative level of PRM2 to be reduced, and PRM2 aberrantly located in the cytoplasm and residual bodies of condensing/condensed spermatids in the testis, we next evaluated the histone-to-protamine transition. To this end, we performed IHC staining to detect histone H3, transition protein 1 (TNP1) and PRM1 in testis and epididymis sections. In $Prm2^{\Delta c/+}$ male mice PRM1 staining intensity and localization is comparable to the WT. However, PRM1 staining seems to be lost in $Prm2^{\Delta c/-}$ sperm from cauda epididymis (Fig. S6, Fig. 5). This is most likely due to the strong degradation of the sperm and its DNA and low sperm count in this genotype. We did not find any apparent increase in total histone H3 signal (Fig. S6, Fig. 5), However, in contrast to WT, TNP1 was retained in both $Prm2^{\Delta c/+}$ and $Prm2^{\Delta c/-}$ males in step 15-16 spermatids and caput epididymal sperm. In cauda epididymal sperm however, we did not find any visible signal of TNP1 (Fig. S6, Fig. 5). This indicates, that loss of cP2 leads to transition protein retention.

In order to further investigate histone retention and alteration in nuclear protein content we performed mass spectrometric analysis on mature sperm basic nuclear protein extracts and analyzed differential abundance (DA) of the detected proteins. Compared to wildtype, we found 14 proteins to be DA in $Prm2^{\Delta c/+}$ sperm, 20 in $Prm2^{\Delta c/-}$ males and 24 for $Prm2^{-/-}$ sperm. Seven proteins were DA in all three comparisons, several of those associated with stress response and/or apoptosis (HSPA2, B2M, CLU) (Fig. 6A,B). Consistent with IHC results we did not find any histones that were significantly higher abundant in $Prm2^{\Delta c/+}$ or $Prm2^{\Delta c/-}$ males. We therefore conclude that histone retention is not increased in males harboring the $Prm2^{\Delta c}$ allele. Interestingly in the $Prm2^{-/-}$ samples we did find histones (H3f3, H3C, H4C) to be

significantly higher abundant, indicating increased histone retention when PRM2 is completely lacking. Transition proteins were not detected. Lists of DA proteins including statistics can be found in supplementary dataset S2.

Eight proteins were not DA in $Prm2^{-/-}$ compared to WT, but in $Prm2^{\Delta c/+}$ and/or $Prm2^{\Delta c/-}$ males. Of these, RPL26 and GSTM5 are involved in DNA damage response and/or oxidative stress pathways, while TUBA3B and ANT4 (*Slc25a31*) are related to motility. Of note, citrate synthase (CS) is specifically higher abundant in $Prm2^{\Delta c/+}$ and $Prm2^{\Delta c/-}$ males. Most interestingly, we found the histone H2A variant H2A.L.2 to be significantly lower abundant in $Prm2^{\Delta c/-}$ males, compared to the wildtype (Fig. 6A-D). H2A.L.2 is a spermatid/sperm-specific histone variant and a key player in histone-to-protamine transition. Together with TH2B it forms a nucleosome with an open chromatin structure allowing for loading of transition proteins followed by protamine recruitment and histone and transition protein eviction by protamines (Barral et al. 2017) (Fig. 6D). According to Hoghoughi et al. (2020) H2A.L.2 is retained in mature sperm in pericentric heterochromatin. We therefore investigated the presence and co-localization of H2A.L.2 and PRM2 in $Prm2^{\Delta c/-}$ and $Prm2^{\Delta c/+}$ males, by immunofluorescent staining of condensed step 15-16 spermatids from tubule preparations and mature sperm extracted from the cauda epididymis. In the wildtype, we found a moderately strong signal for H2A.L.2 in the pericentric region of the nucleus, with PRM2 signal in the whole nucleus (Fig. 7a-b,g-h). However, in $Prm2^{\Delta c/+}$ and $Prm2^{\Delta c/-}$ step 15-16 spermatids the H2A.L.2 signal is stronger compared to the WT and localized in DAPI-bright foci in the nucleus (Fig. 7c-f). DAPI-bright regions in nuclei usually correspond to heterochromatin. In mature sperm, however, the H2A.L.2 signal is almost completely lost in $Prm2^{\Delta c/+}$ and $Prm2^{\Delta c/-}$ males, consistent with the lower abundance found in mass spectrometric analysis. The PRM2 signal is diffuse and distributed along the whole mature sperm cell, likely due to severe membrane damage and degradation (Fig. 7i-l).

Discussion

The crucial role of protamines in the process of sperm chromatin reorganization is well known. However, why two protamines are needed in some species, while PRM1 seems to be sufficient in others is still unclear. The main difference between PRM1 and PRM2 is the highly conserved N-terminal cleaved PRM2 domain (cP2). Its function remains elusive to date. Using gene-editing we generated mice lacking the cleaved-*Prm2* (cP2) domain. We show that the cP2 domain is indispensable for PRM2 function and required for male mouse fertility. Mice heterozygous for the deletion of the domain display inviable and immotile sperm. Loss of cP2 leads to severe retention of transition proteins and reduced incorporation of PRM2 into nucleoprotamine. Instead, mature-PRM2 (mP2) is aberrantly found in spermatid cytoplasm and residual bodies. While overall histone retention is not increased, the histone variant H2A.L.2 is less abundant in mature sperm deficient in cP2.

Firstly, mP2 expressed from the $Prm2^{\Delta c}$ allele was detected in the nucleus of condensed spermatids of cP2 deficient mice and was shown to be able to condense somatic cell DNA *in-vitro* similar to PRM2, or PRM1 (Iuso et al. 2015). We therefore conclude that the mP2 domain produced by gene editing seems to maintain its main function during spermiogenesis in cP2 deficient mouse lines. Male $Prm2^{\Delta c/+}$ mice are infertile, show complete fragmentation of mature sperm DNA, loss of viability and immotility of mature sperm. This is in contrast to $PRM2^{+/-}$ males, which remained fertile (Schneider et al. 2016). In order to test, whether the infertility of $Prm2^{\Delta c/+}$ mice is due to an aberrant interaction between mP2 and the wildtype PRM2 precursor, we bred the $Prm2^{\Delta c}$ allele with the $Prm2^{\Delta 97bp}$ mouse line generated and analyzed by Schneider et al. (2016, 2020). However, mice expressing only mP2 ($Prm2^{\Delta c/-}$) were also infertile showing an even more extreme phenotype than $Prm2^{\Delta c/+}$ males. Since $Prm2^{+/-}$ male mice are reported to be fertile, these data clearly indicate, that loss of cP2 leads to male infertility in mice. We speculate, that this holds also true for all other species which harbor a functional PRM2 gene.

Since mature sperm chromatin is completely fragmented in cP2 deficient males and mature sperm are inviable and immotile similar to $Prm2^{-/-}$ sperm, we suspected that sperm might undergo epididymal degradation mediated by oxidative stress. Schneider et al. (2020)

showed that loss of PRM2 seems to lead to reduced antioxidant capacity of sperm, initiating an oxidative stress-mediated destruction cascade during epididymal transit. Indeed, cP2 deficient mice showed a strong increase in oxidative DNA damage in the cauda epididymis. Prm2$^{\Delta C/-}$ sperm seem to be degraded to an extent that many of the caudal sperm are completely disintegrated, leading to a significantly reduced sperm count. We propose that this is not a specific effect of cP2 or PRM2 deficiency but an inherent epididymal mechanism evoked by DNA damage or aberrant protamination (or even otherwise damaged sperm, e.g.: membrane defects, aberrant morphology or sperm surface proteome). How sperm damage might be sensed by epididymal cells and what, in fact, initiates this cascade is an interesting avenue for further investigation.

Given the timing of *Prm2* expression and processing, the primary effects of cP2 loss are likely to be found during the transition from histone-bound to protaminized DNA in the final stages of spermiogenesis. Barral et al. (2017) describe this transition taking place by assembly of a histone (TH2B and H2A.L.2) - transition protein (TNP1 and TNP2) interface followed by protamine recruitment and processing. Protamines themselves subsequently replace histones. This process is disrupted in cP2 deficient mice.

Firstly, in cP2 deficient mice mP2 is detected in the cytoplasm and residual bodies in addition to the signal found in the nucleus, indicating that mP2 is not completely incorporated into the condensing chromatin. In consequence, the protamine ratio changes from 2:1 in wildtype to 1:2-1:5 in cP2 deficient sperm. This indicates, that the cP2 domain facilitates incorporation of PRM2 and assembly of nucleoprotamine.

Secondly, we found retention of TNP1 in condensed testicular spermatids and caput epididymal sperm, indicating that the eviction of TNP1 is hampered due to the loss of cP2 or that TNP1 is binding DNA in a competitive manner. Of note, a recent study investigating a single residue mutation in PRM1 showed increased histone retention, but no disturbances in transition protein retention in such mice (Moritz et al. 2021). Transition proteins are believed to aid in chromatin condensation by stabilizing the DNA in a non-supercoiled state, cooperating with topoisomerases to relieve torsional stress and to be involved in DNA repair

530 during chromatin condensation (Singh and Rao, 1988 Lèvesque et al. 1998, Akama et al.
531 1999). Loss of either transition protein results in incomplete PRM2 processing (Yu et al.
532 2000, Shirley et al. 2004, Zhao et al. 2004) and TNP2 was shown to interact with PRM2
533 (Barral et al. 2017). This demonstrates that transition proteins are required for proper PRM2
534 processing during nucleoprotamine assembly. The fact that we find severe retention of TNP1
535 in condensed spermatids indicates, that the cP2 domain in turn, is required for the proper
536 processing (i.e. eviction) of TNP1.

537 Surprisingly, however, overall histone retention was not increased. This was
538 confirmed by H3 immunostaining and mature sperm basic nuclear protein abundance
539 analysis. Interestingly, we do find an increased retention of H3 and H4 variants in $Prm2^{-/-}$
540 deficient sperm. The data from the H3 immunostainig indicate, that the global amount of
541 retained histones seems unaffected, and hence not controlled by protamine ratio or PRM2
542 processing.

543 The retention of transition protein detected in cP2 deficient mice seems to go along
544 with altered retention of H2A.L.2. During the first steps of chromatin condensation H2A.L.2,
545 together with TH2B provides an open chromatin interface necessary for transition protein
546 loading. Barral et al. (2017) showed, that deletion of H2A.L.2 leads to infertility, aberrant
547 transition protein loading and disturbed processing of PRM2. In mature sperm H2A.L.2 was
548 shown to be retained in pericentric heterochromatin (Govin et al. 2007, Hoghoughi et al.
549 2020). This retention seems to be lost in $Prm2^{\Delta C/-}$ mature sperm, where H2A.L.2 was shown
550 to be significantly lower abundant. However, a strong H2A.L.2 signal can be observed in
551 $Prm2^{\Delta C/-}$ condensed spermatids in the testis, were it overlaps with atypical speckles of bright
552 DAPI signal. Thus, it seems that H2A.L.2-transition protein complexes are retained in
553 aberrant clumps of heterochromatin in cP2 deficient mice.

554 Protamines have a strong electrostatic attraction to DNA due to arginine clusters
555 (Moritz et al. 2021). This allows protamines to condense DNA even in the absence of
556 spermatid specific histones and transition proteins, as shown in *in-vitro* assays in somatic
557 cells and in this study (Iuso et al. 2015). However, uncontrolled or unbalanced binding of

protamines might lead to strong torsional stress and DNA damage. A controlled stepwise chromatin condensation therefore could be required to maintain chromatin integrity. Moritz et al. (2021) recently showed that the PRM2 precursor has a lower DNA binding affinity than mP2, leading to faster DNA condensation by mP2. Barral et al. (2017) suggested that transition proteins buffer protamine incorporation by allowing for ordered protamine loading and (or possibly through) PRM2 processing. By losing the cP2 domain this processing step is skipped. We therefore propose, that the aberrant interaction with transition proteins due to cP2 deficiency leads to random mP2 binding, leading to strong hypercondensation of open chromatin resulting in DNA strand breaks. Transition protein-loaded chromatin, however does not allow for mP2 loading, leading to incomplete mP2 incorporation and retention of H2A.L.2 – transition protein complexes in aberrantly located heterochromatin foci, that are lost by DNA degradation during epididymal transit.

In conclusion, our results show that the cleaved domain of PRM2 is essential for sperm function and fertility. Loss of the domain leads to incomplete protamination, a switch in the protamine ratio and transition protein retention in epididymal sperm. During epididymal transit cP2 deficient sperm are degraded, seemingly by ROS mediated damage, leading to complete DNA fragmentation. cP2 seems to be necessary for correct interaction between the H2A.L.2 - transition protein complex and PRM2. We were able to provide a first glimpse into the function of cleaved PRM2 and PRM2 processing, that opens up multiple avenues for further investigation.

Acknowledgments: This study was supported by grants from the Deutsche Forschungsgemeinschaft (DFG) to L.A. (AR 1221/1-1) and H.S. (Scho 503/15-2). L.A. was further supported by the University of Bonn Medical school supplementary research grant program *FEMHABIL*. We thank Gaby Beine, Angela Egert and Andrea Jäger for excellent technical assistance. Protein identifications were done at the Core Facility Mass Spectrometry, Institute of Biochemistry and Molecular Biology, Medical Faculty, University of Bonn. Mass spectrometer funded by the Deutsche Forschungsgemeinschaft (DFG) –

Projektnummer 386936527. RNAseq was done at University of Bonn Core facility for Next Generation Sequencing (NGS). We thank Saadi Khochbin and Sophie Barral for the gift of the H2A.L.2 antibody and excellent advice.

Author contributions: L.A. and H.S. conceived the study and designed the experiments. L.A. and S.S. generated gene-edited mice. L.A. and G.E.M. analysed gene-edited mice. F.E.O. and I.N. generated IHC stainings. L.A. and H.S. drafted the manuscript. All authors read and approved the final manuscript.

References

Ahlmann-Eltze C, Anders S. proDA: Probabilistic dropout analysis for identifying differentially abundant proteins in label-free mass spectrometry. Biorxiv. 2020; 1:661496.

Akama K, Kondo M, Sato H, Nakano M. Transition protein 4 from boar late spermatid nuclei is a topological factor that stimulates DNA-relaxing activity of topoisomerase I. FEBS letters. 1999; 442:189-92.

Aoki VW, Liu L, Jones KP, Hatasaka HH, Gibson M, Peterson CM, Carrell DT. Sperm protamine 1/protamine 2 ratios are related to in vitro fertilization pregnancy rates and predictive of fertilization ability. Fertility and Sterility. 2006; 86:1408-15.

Balhorn R. Mammalian Proteins: structure and Molecular Interaction. In: Adolph KW, editor. Molecular Biology of Chromosome Function. New York: Springer Verlag; 1989. pp. 366–395.

Balhorn R. The protamine family of sperm nuclear proteins. Genome Biol. 2007; 227. doi:10.1186/gb-2007-8-9-227

Barral S, Morozumi Y, Tanaka H, Montellier E, Govin J, de Dieuleveult M, et al. Histone Variant H2A.L.2 Guides Transition Protein-Dependent Protamine Assembly in Male Germ Cells. Mol Cell. 2017; 89–101.e8. doi:10.1016/j.molcel.2017.02.025

612 Chauviere M, Martinge A, DeBarle M, Sautiere P, Chevallier P. Molecular characterization of
613 six intermediate proteins in the processing of mouse protamine P2 precursor. Eur J
614 Biochem. 1992; 759–765. doi:10.1111/j.1432-1033.1992.tb16691.x
615 Chen H, Cheung MPL, Chow PH, Cheung ALM, Liu W, O WS. Protection of sperm DNA
616 against oxidative stress in vivo by accessory sex gland secretions in male hamsters.
617 Reproduction. 2002; 491–499.
618 Corzett M, Mazrimas J, Balhorn R. Protamine 1: Protamine 2 stoichiometry in the sperm of
619 eutherian mammals. Mol Reprod Dev. 2002; 519–527. doi:10.1002/mrd.10105
620 de Mateo S, Gázquez C, Guimerà M, Balasch J, Meistrich ML, Ballescà JL, Oliva R.
621 Protamine 2 precursors (Pre-P2), protamine 1 to protamine 2 ratio (P1/P2), and assisted
622 reproduction outcome. Fertility and sterility. 2009; 91:715-22.
623 de Mateo S, Ramos L, de Boer P, Meistrich M, Oliva R. Protamine 2 precursors and
624 processing. Protein and peptide letters. 2011; 18:778-85.
625 de Yebra L, Ballescá JL, Vanrell JA, Corzett M, Balhorn R, Oliva R. Detection of P2
626 precursors in the sperm cells of infertile patients who have reduced protamine P2 levels.
627 Fertil Steril. 1998; 755–9.
628 García-Peiró A, Martínez-Heredia J, Oliver-Bonet M, Abad C, Amengual MJ, Navarro J,
629 Jones C, Coward K, Gosálvez J, Benet J. Protamine 1 to protamine 2 ratio correlates with
630 dynamic aspects of DNA fragmentation in human sperm. Fertility and sterility. 2011;
631 95:105-9.
632 Govin J, Escoffier E, Rousseaux S, Kuhn L, Ferro M, Thévenon J, Catena R, Davidson I,
633 Garin J, Khochbin S, Caron C. Pericentric heterochromatin reprogramming by new
634 histone variants during mouse spermiogenesis. The Journal of cell biology. 2007;
635 176:283-94.
636 Hada M, Masuda K, Yamaguchi K, Shirahige K, Okada Y. Identification of a variant-specific
637 phosphorylation of TH2A during spermiogenesis. Sci Rep. 2017; 46228.
638 doi:10.1038/srep46228

639 Hoghoughi N, Barral S, Curtet S, Chuffart F, Charbonnier G, Puthier D, Buchou T,
640 Rousseaux S, Khochbin S. RNA-Guided genomic localization of H2A. L. 2 histone variant.
641 Cells. 2020; 9:474.
642 Ishibashi T, Li A, Eirín-López JM, Zhao M, Missiaen K, Abbott DW, Meistrich M, Hendzel MJ,
643 Ausio J. H2A. Bbd: an X-chromosome-encoded histone involved in mammalian
644 spermiogenesis. Nucleic acids research. 2010; 38:1780-9.
645 Iuso D, Czernik M, Toschi P, Fidanza A, Zacchini F, Feil R, Curtet S, Buchou T, Shiota H,
646 Khochbin S, Ptak GE. Exogenous expression of human protamine 1 (hPrm1) remodels
647 fibroblast nuclei into spermatid-like structures. Cell reports. 2015; 13:1765-71.
648 Käll L, Storey JD, MacCoss MJ, Noble WS. Assigning significance to peptides identified by
649 tandem mass spectrometry using decoy databases. Journal of proteome research. 2008;
650 7:29-34.
651 Kim D, Langmead B, Salzberg S L. HISAT: A fast spliced aligner with low memory
652 requirements. Nat Methods. 2015; 12:357–360.
653 Kotaja N, Kimmins S, Brancorsini S, Hentsch D, Vonesch JL, Davidson I, Parvinen M,
654 Sassone-Corsi P. Preparation, isolation and characterization of stage-specific
655 spermatogenic cells for cellular and molecular analysis. Nature methods. 2004;1:249-54.
656 Krawetz SA, Dixon GH. Sequence similarities of the protamine genes: Implications for
657 regulation and evolution. J Mol Evol. 1988; 291–297. doi:10.1007/BF02101190
658 Lévesque D, Veilleux S, Caron N, Boissonneault G. Architectural DNA-binding properties of
659 the spermatidal transition proteins 1 and 2. Biochemical and biophysical research
660 communications. 1998; 252:602-9.
661 Love M I, Huber W, Anders S. 2014. Moderated estimation of fold change and dispersion for
662 RNA-seq data with DESeq2. Genome Biol. 2014; 15:1–21.
663 Lüke L, Campbell P, Varea Sánchez M, Nachman MW, Roldan ERS. Sexual selection on
664 protamine and transition nuclear protein expression in mouse species. Proc Biol Sci.
665 2014; 20133359. doi:10.1098/rspb.2013.3359

666 Lüke L, Tourmente M, Roldan ERS. Sexual selection of protamine 1 in mammals. Mol Biol
667 Evol. 2016; 174–184. doi:10.1093/molbev/msv209
668 Lüke L, Vicens A, Serra F, Luque-Larena JJ, Dopazo H, Roldan ERS, et al. Sexual Selection
669 Halts the Relaxation of Protamine 2 among Rodents. PLoS One. 2011; e29247.
670 doi:10.1371/journal.pone.0029247
671 Lüke L, Vicens A, Tourmente M, Roldan ERS. Evolution of protamine genes and changes in
672 sperm head phenotype in rodents. Biol Reprod. 2014; 67.
673 doi:10.1095/biolreprod.113.115956
674 Mellacheruvu D, Wright Z, Couzens AL, Lambert JP, St-Denis NA, Li T, Miteva YV, Hauri S,
675 Sardiu ME, Low TY, Halim VA. The CRAPome: a contaminant repository for affinity
676 purification–mass spectrometry data. Nature methods. 2013; 10:730-6.
677 Mi H, Huang X, Muruganujan A, Tang H, Mills C, Kang D, Thomas PD. 2017. PANTHER
678 version 11: Expanded annotation data from Gene Ontology and Reactome pathways, and
679 data analysis tool enhancements. Nucleic Acids Res. 2017; 45:D183–D189.
680 Moritz L, Schon S, Rabbani M, Sheng Y, Pendlebury D, Agrawal R, Sultan C, Jorgensen K,
681 Zheng X, Diehl A, Ragunathan K. Single residue substitution in protamine 1 disrupts
682 sperm genome packaging and embryonic development in mice. bioRxiv. 2021.
683 Oliva R, Dixon GH. Vertebrate protamine genes and the histone-to-protamine replacement
684 reaction. Biology WEC and KMBT-P in NAR and M, editor. Prog Nucleic Acid Res Mol
685 Biol; 1991; 25–94.
686 Pertea M, Pertea GM, Antonescu CM, Chang TC, Mendell JT, Salzberg SL. 2015. StringTie
687 enables improved reconstruction of a transcriptome from RNA-seq reads. Nat Biotechnol.
688 2015; 33:290–295.
689 Piunti A, Shilatifard A. The roles of Polycomb repressive complexes in mammalian
690 development and cancer. Nature Reviews Molecular Cell Biology. 2021; 22:326-45.
691 Rathke C, Baarends WM, Awe S, Renkawitz-Pohl R. Chromatin dynamics during
692 spermiogenesis. Biochimica et Biophysica Acta - Gene Regulatory Mechanisms. 2014;
693 155–168. doi:10.1016/j.bbagrm.2013.08.004

694 Retief JD, Dixon GH. Evolution of pro-protamine P2 genes in primates. Eur J Biochem. 1993;
695 609–615. doi:10.1111/j.1432-1033.1993.tb17960.x
696 Retief JD, Winkfein RJ, Dixon GH, Adroer R, Queralt R, Ballabriga J, et al. Evolution of
697 Protamine P1 Genes in Primates. J Mol Evol. 1993; 426–434.
698 Robinson JT, Thorvaldsdóttir H, Winckler W, Guttman M, Lander ES, Getz G, Mesirov JP.
699 Integrative genomics viewer. Nature biotechnology. 2011; 29:24-6.
700 Ruiz-Lopez MJ, Espeso G, Evenson DP, Roldan ERS, Gomendio M. Paternal levels of DNA
701 damage in spermatozoa and maternal parity influence offspring mortality in an
702 endangered ungulate. Proc R Soc B Biol Sci. 2010; 2541–2546.
703 doi:10.1098/rspb.2010.0333
704 Schneider S, Shakeri F, Trötschel C, Arévalo L, Kruse A, Buness A, Poetsch A, Steger K,
705 Schorle H. Protamine-2 deficiency initiates a reactive oxygen species (ROS)-mediated
706 destruction cascade during epididymal sperm maturation in mice. Cells. 2020; 9:1789.
707 Schneider S, Balbach M, Jan F. Jikeli, Fietz D, Nettersheim D, Jostes S, et al. Re-visiting the
708 Protamine-2 locus: deletion, but not haploinsufficiency, renders male mice infertile. Sci
709 Rep. 2016; 36764. doi:10.1038/srep36764
710 Shirley CR, Hayashi S, Mounsey S, Yanagimachi R, Meistrich ML. Abnormalities and
711 reduced reproductive potential of sperm from Tnp1-and Tnp2-null double mutant mice.
712 Biology of reproduction. 2004;71:1220-9.
713 Singh J, Rao MRS. Interaction of rat testis protein, TP, with nucleosome core particle.
714 Biochem Int. 1988; 17:701–710
715 Skinner BM, Rathje CC, Bacon J, Johnson EE, Larson EL, Kopania EE, Good JM, Yousafzai
716 G, Affara NA, Ellis PJ. A high-throughput method for unbiased quantitation and
717 categorization of nuclear morphology. Biology of reproduction. 2019; 100:1250-60.
718 Soler-Ventura A, Castillo J, de la Iglesia A, Jodar M, Barrachina F, Ballesca JL, Oliva R.
719 Mammalian sperm protamine extraction and analysis: a step-by-step detailed protocol and
720 brief review of protamine alterations. Protein and peptide letters. 2018; 25:424-33.

721 Steger K, Wilhelm J, Konrad L, Stalf T, Greb R, Diemer T, Kliesch S, Bergmann M, Weidner
722 W. Both protamine-1 to protamine-2 mRNA ratio and Bcl2 mRNA content in testicular
723 spermatids and ejaculated spermatozoa discriminate between fertile and infertile men.
724 Human Reproduction. 2008; 23:11-6.
725 Tanaka H, Baba T. Gene expression in spermiogenesis. Cell Mol Life Sci. 2005; 344–354.
726 doi:10.1007/s00018-004-4394-y
727 Torregrosa N, Domínguez-Fandos D, Camejo MI, Shirley CR, Meistrich ML, Ballescà JL, et
728 al. Protamine 2 precursors, protamine 1/protamine 2 ratio, DNA integrity and other sperm
729 parameters in infertile patients. Hum Reprod. 2006; 2084–9. doi:10.1093/humrep/del114
730 Tourmente M, Gomendio M, Roldan ERS. Sperm competition and the evolution of sperm
731 design in mammals. BMC Evol Biol. 2011; 12. doi:10.1186/1471-2148-11-12
732 Wickham H. ggplot2. Wiley Interdisciplinary Reviews: Computational Statistics. 2011; 3:180-
733 5.
734 Yelick P, Balhorn ROD, Johnson PA, Corzett M, Mazrimas JOEA, Kleene KKC, et al. Mouse
735 protamine 2 is synthesized as a precursor whereas mouse protamine 1 is not. Mol Cell
736 Biol. Am Soc Microbiol; 1987; 2173. doi:10.1128/MCB.7.6.2173.
737 Yu YE, Zhang Y, Unni E, Shirley CR, Deng JM, Russell LD, Weil MM, Behringer RR,
738 Meistrich ML. Abnormal spermatogenesis and reduced fertility in transition nuclear protein
739 1-deficient mice. Proceedings of the National Academy of Sciences. 2000; 97:4683-8.
740 Zatecka E, Castillo J, Elzeinova F, Kubatova A, Ded L, Peknicova J, Oliva R. The effect of
741 tetrabromobisphenol A on protamine content and DNA integrity in mouse spermatozoa.
742 Andrology. 2014; 2:910-7.
743 Zhao M, Shirley CRCR, Yu YEE, Mohapatra B, Zhang YUN, Unni E, et al. Targeted
744 disruption of the transition protein 2 gene affects sperm chromatin structure and reduces
745 fertility in mice. Mol Cell Biol. 2001; 7243. doi:10.1128/MCB.21.21.7243
746 Zhao M, Shirley CR, Mounsey S, Meistrich ML. Nucleoprotein transitions during
747 spermiogenesis in mice with transition nuclear protein Tnp1 and Tnp2 mutations. Biology
748 of reproduction. 2004; 71:1016-25.

Figure legends

Figure 1. Gene editing, fertility and expression. A) Schematic representation of the generation of cP2 deletion. Double strand breaks induced by Cas9 indicated by black triangles. B) Schematic overview of analyzed genotypes and fertility. $Prm2^{+/-}$ and $Prm2^{-/-}$ (Schneider et al. 2016) were included as a comparison. Barplot of average litter size for WT, $Prm2^{+/-}$, $Prm2^{-/-}$, $Prm2^{\Delta c/+}$ and $Prm2^{\Delta c/-}$, n=5 for each genotype. C) Barplot showing average DESeq2 normalized read counts of *Prm2* for WT, $Prm2^{\Delta c/+}$ and $Prm2^{\Delta c/-}$. D) Barplot showing comparison between number of differentially higher and lower expressed genes for $Prm2^{\Delta c/+}$ and $Prm2^{\Delta c/-}$ compared to wildtype.

Figure 2. Localization and DNA condensing ability of mP2. A) Immunohistochemical fluorescent staining of PRM2 (WT, $Prm2^{\Delta c/+}$) or mP2 ($Prm2^{\Delta c/+}$, $Prm2^{\Delta c/-}$) (green) in testis sections, counterstaining with DAPI (blue). Scale bar = 50µm. B) Heterologous expression of plasmids encoding eGFP tagged PRM2 (*Prm2*-eGFP) or mP2 (*mP2*-eGFP) in human embryonic kidney 293 (HEK) cells 48 hours post-transfection. Scale bar = 10µm.

Figure 3. Sperm and testis parameters and histology. A) Barplots showing data for relative testes mass, mature sperm count, percentage of viable mature sperm (eosin-nigrosin assay) and percentage of motile mature sperm in $Prm2^{\Delta c/+}$ and $Prm2^{\Delta c/-}$ mice compared to wildtype. B) PAS staining of testis and epididymal sections of $Prm2^{\Delta c/+}$, $Prm2^{\Delta c/-}$ and WT males. Scale bar = 50µm (200µm for left column).

Figure 4. Chromatin integrity, nuclear morphology and protamine content. A) Agarose gel of DNA extracted from WT, $Prm2^{+/-}$, $Prm2^{-/-}$ and $Prm2^{\Delta c/+}$ mature sperm. B) Immunohistochemical fluorescent staining of 8-Oxo-2'-deoxyguanosine (8-OHdG) (green) in caput epididymis (upper row) and cauda epididymis (lower row) of $Prm2^{\Delta c/+}$, $Prm2^{\Delta c/-}$ and WT. Counterstained with DAPI (pseudo-colored grey). Scale bar = 50µm. C) Comparison of

777 mature sperm nucleus consensus shapes of WT, Prm2$^{+/-}$, Prm2$^{-/-}$, Prm2$^{\Delta c/+}$ and Prm2$^{\Delta c/-}$
778 resulting from nuclear morphology analysis. Numbers inside the consensus shapes indicate
779 the number of nuclei assessed and assigned to the respective consensus shape cluster.
780 Upper row shows the consensus shape of the different gene edited lines overlaid with the
781 wildtype consensus shape. cl. = cluster. D) Representative lanes of acid-urea gel
782 electrophoresis (AU-PAGE) of WT, Prm2$^{+/-}$, Prm2$^{-/-}$, Prm2$^{\Delta c/+}$ and Prm2$^{\Delta c/-}$ mature sperm
783 basic nuclear protein extractions. a=non-protamine basic nuclear proteins, b=PRM2
784 precursors, open arrowhead indicates mature PRM2 band, solid arrowhead indicates PRM1
785 band. To the right: quantification of the percentage of PRM2 (including PRM2 precursors) of
786 total protamine by band density analysis. Asterisk indicates significant difference.
787
788 **Figure 5.** Histone H3, transition protein 1 and protamine 1 staining. Two left columns:
789 Immunohistochemical fluorescent staining of Histone H3 (H3) (red) and protamine 1 (PRM1)
790 (green) in WT, Prm2$^{\Delta/+}$ and Prm2$^{\Delta/-}$ caput epididymis. Counterstained with DAPI (blue). Scale
791 bar = 50µm. Columns to the right: Immunohistochemical fluorescent staining of transition
792 protein 1 (TNP1) (red) and protamine 1 (PRM1) (green) in WT, Prm2$^{\Delta/+}$ and Prm2$^{\Delta/-}$ caput
793 and cauda epididymis. Counterstained with DAPI (blue). Scale bar = 50µm.
794
795 **Figure 6.** Differential abundance of mature sperm basic nuclear proteins. A) volcano plots
796 showing differential abundance (DA) of basic nuclear proteins in Prm2$^{\Delta/+}$ compared to WT
797 (upper plot) and Prm2$^{\Delta/-}$ compared to WT (lower plot). Significantly DA proteins are indicated
798 in color (teal = lower abundant, yellow = higher abundant). Top DA proteins and proteins of
799 interest are labeled with their corresponding gene symbol. B) Venn diagram showing the
800 overlap between DA proteins found in the three different comparisons (WT vs. Prm2$^{\Delta/+}$, WT
801 vs. Prm2$^{\Delta/-}$ and WT vs. Prm2$^{-/-}$). Proteins present in overlaps of interest are listed with their
802 corresponding gene symbol. H2A.L.2 is marked in red. C) Boxplot of median normalized log2
803 abundance of H2A.L.2 in WT, Prm2$^{-/-}$, Prm2$^{\Delta/+}$ and Prm2$^{\Delta/-}$. D) Interaction network for
804 H2A.L.2 extracted from String database (Szklarczyk et al. 2019).

805

806 **Figure 7.** Immunohistochemical staining of H2A.L.2 and PRM2. Immunohistochemical
807 fluorescent staining of H2A.L.2 (red) and PRM2 (green) in WT, $Prm2^{\Delta/+}$ and $Prm2^{\Delta/-}$ step 15-
808 16 spermatids from tubule preparations (two left columns) and mature sperm extracted from
809 cauda epididymis (two right columns). Counterstained with DAPI (blue). Scale bar = 20μm.

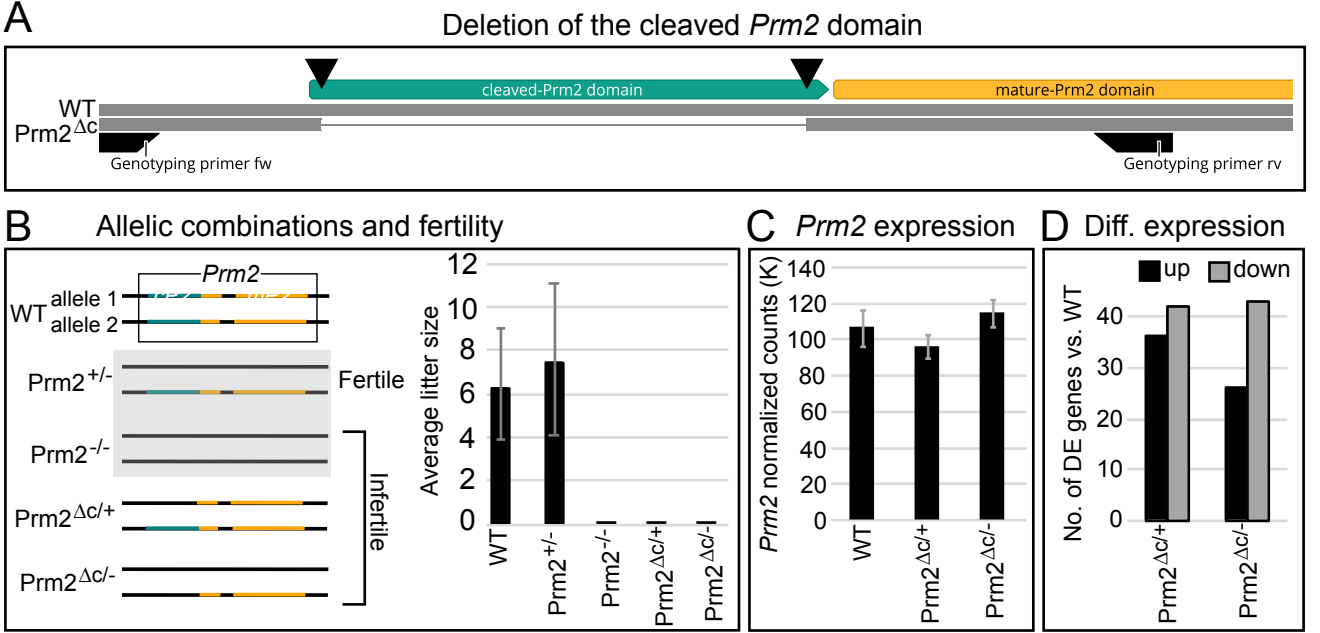
A
Deletion of the cleaved Prm2 domain
cleaved-Prm2 domain
mature-Prm2 domain
WT
Prm2Δc
Genotyping primer fw
Genotyping primer rv
B
Allelic combinations and fertility
Prm2
WT allele 1
allele 2
Prm2+/-
Fertile
Prm2-/-
Infertile
Prm2Δc/+
Prm2Δc/-
Average litter size
12
10
8
6
4
2
0
WT
Prm2+/-
Prm2-/-
Prm2Δc/+
Prm2Δc/-
C
Prm2 expression
Prm2 normalized counts (K)
140
120
100
80
60
40
20
0
WT
Prm2Δc/+
Prm2Δc/-
D
Diff. expression
up
down
No. of DE genes vs. WT
40
30
20
10
0
Prm2Δc/+
Prm2Δc/-

Fig. 1

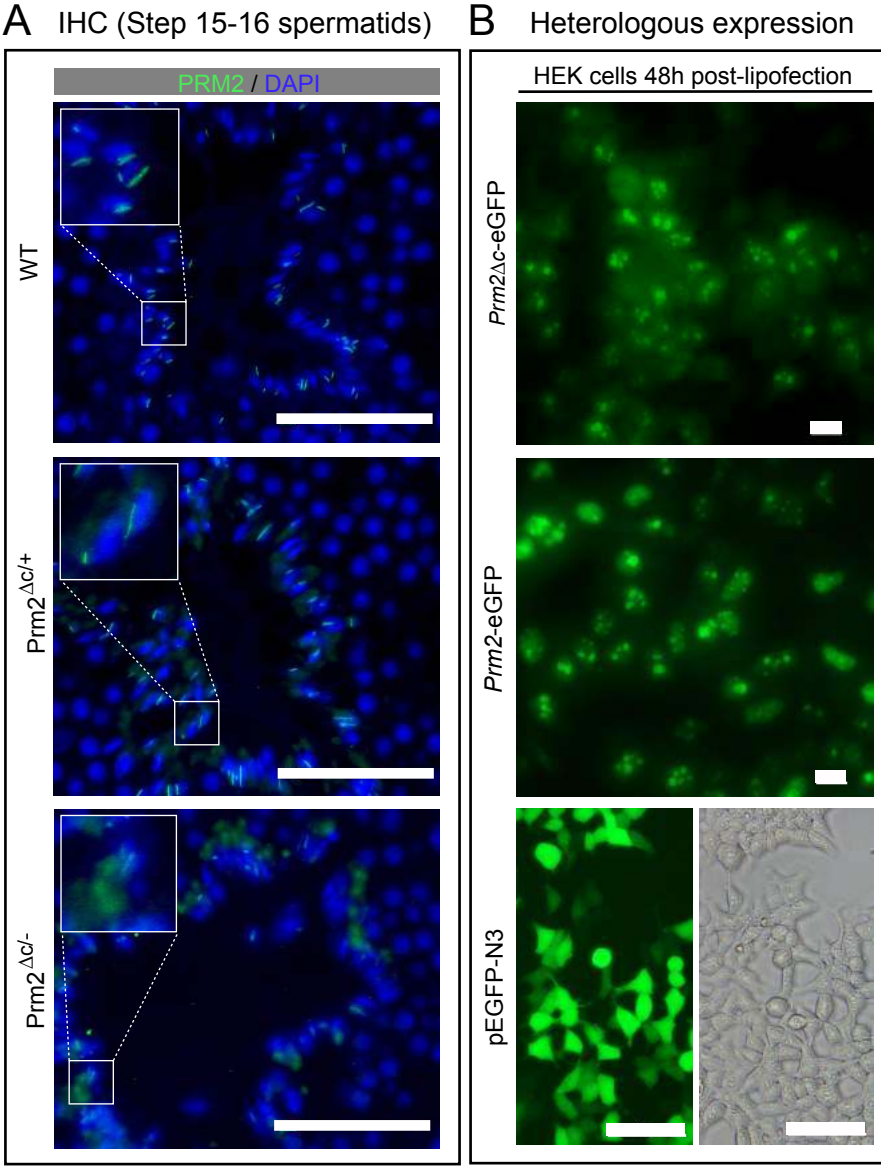
A
IHC (Step 15-16 spermatids)
PRM2 / DAPI
WT
Prm2Δc/+
Prm2Δc/-
B
Heterologous expression
HEK cells 48h post-lipofection
Prm2Δc-eGFP
Prm2-eGFP
pEGFP-N3

Fig. 2

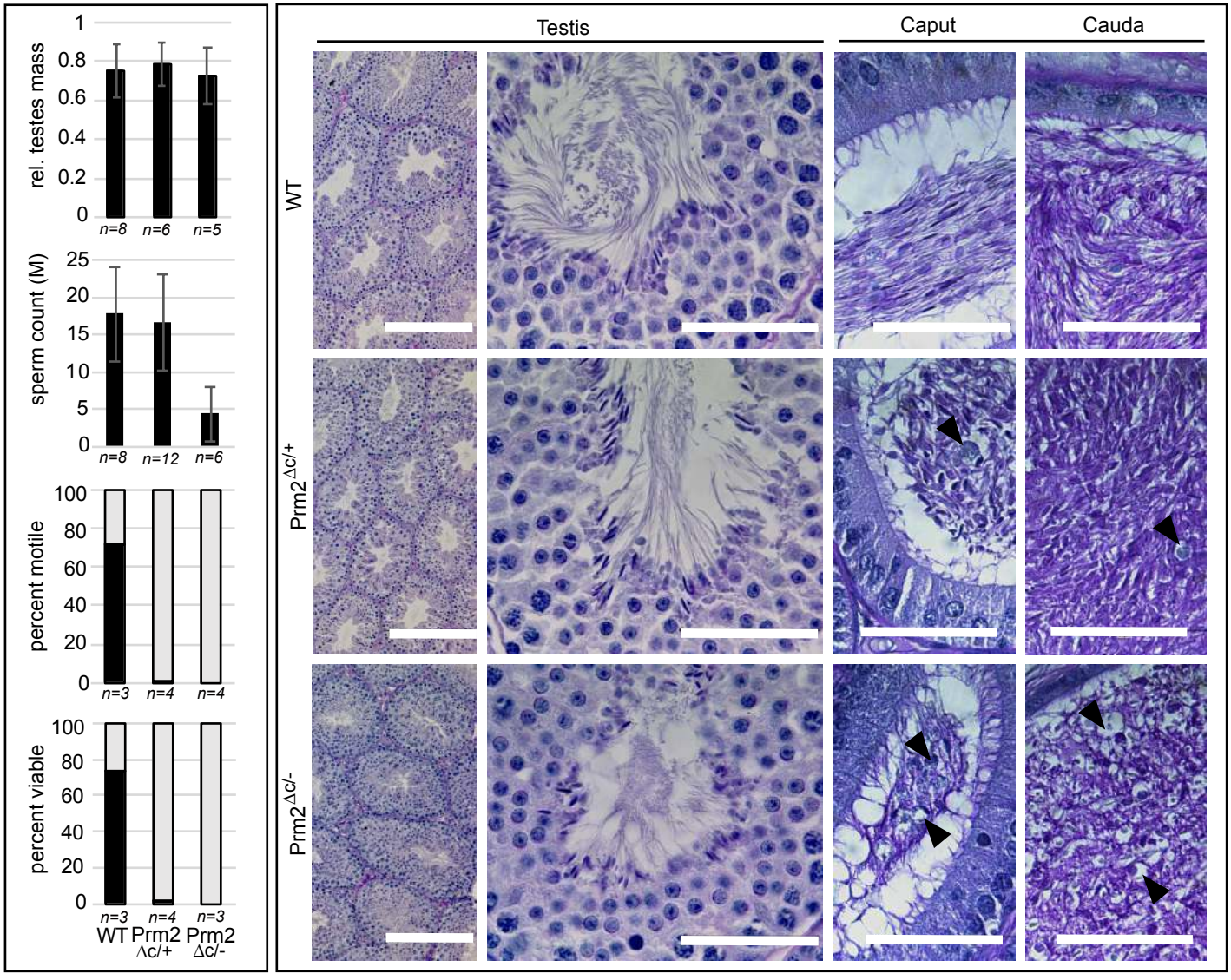
A
Sperm parameters
rel. testes mass
1
0.8
0.6
0.4
0.2
0
n=8
n=6
n=5
sperm count (M)
25
20
15
10
5
0
n=8
n=12
n=6
percent motile
100
80
60
40
20
0
n=3
n=4
n=4
percent viable
100
80
60
40
20
0
n=3
n=4
n=3
WT
Prm2 Δc/+
Prm2 Δc/-
B
Testis histology
Testis
Caput
Cauda
WT
Prm2Δc/+
Prm2Δc/-

Fig. 3

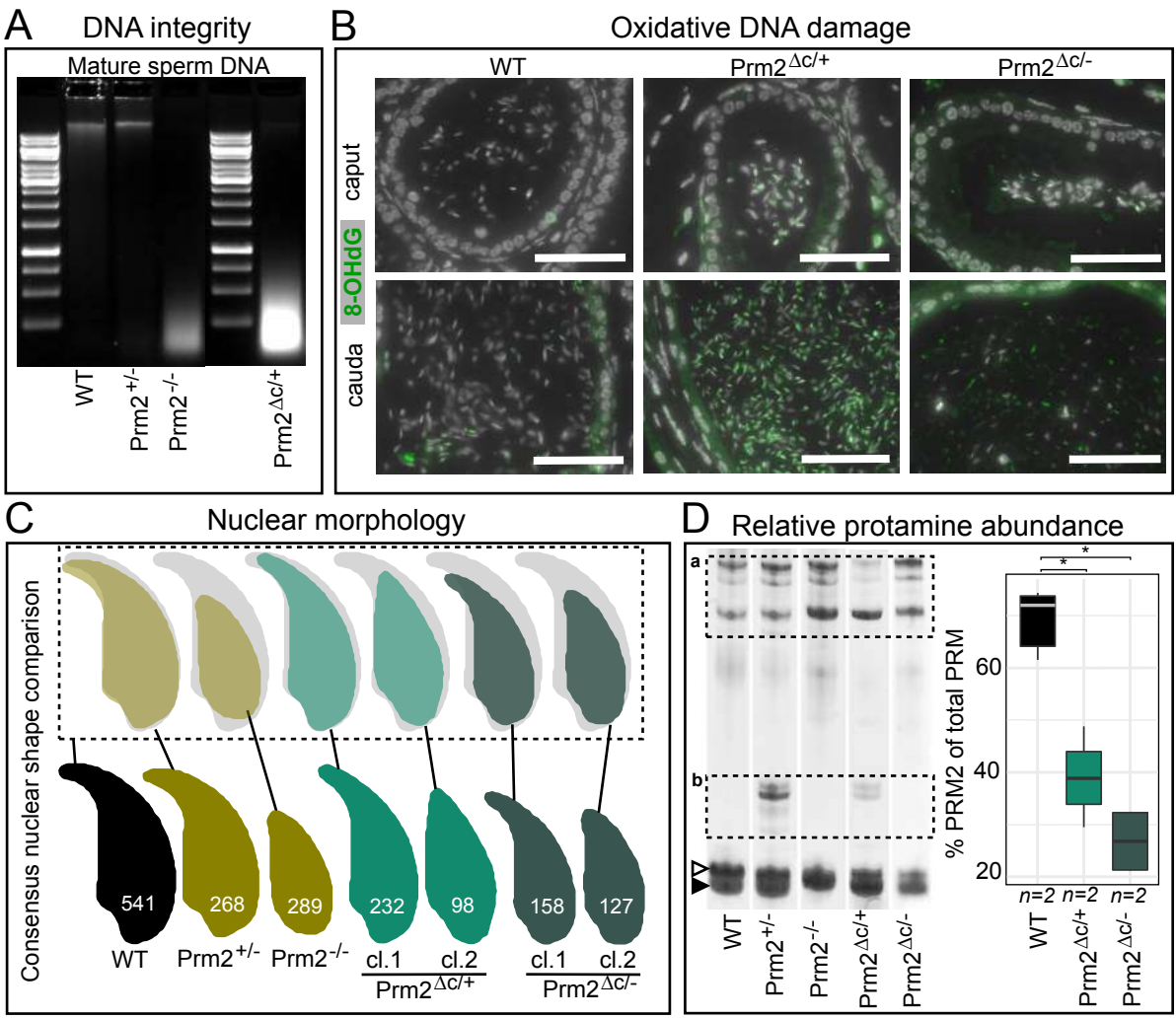
A
DNA integrity
Mature sperm DNA
WT
Prm2+/-
Prm2-/-
Prm2Δc/+
B
Oxidative DNA damage
WT
Prm2Δc/+
Prm2Δc/-
caput
8-OHdG
cauda
C
Nuclear morphology
Consensus nuclear shape comparison
541
268
289
232
98
158
127
WT
Prm2+/-
Prm2-/-
cl.1
cl.2
Prm2Δc/+
cl.1
cl.2
Prm2Δc/-
D
Relative protamine abundance
a
b
WT
Prm2+/-
Prm2-/-
Prm2Δc/+
Prm2Δc/-
% PRM2 of total PRM
60
40
20
n=2
n=2
n=2
WT
Prm2Δc/+
Prm2Δc/-

Fig. 4

Histone H3, Transition protein 1 and Protamine 1 IHC

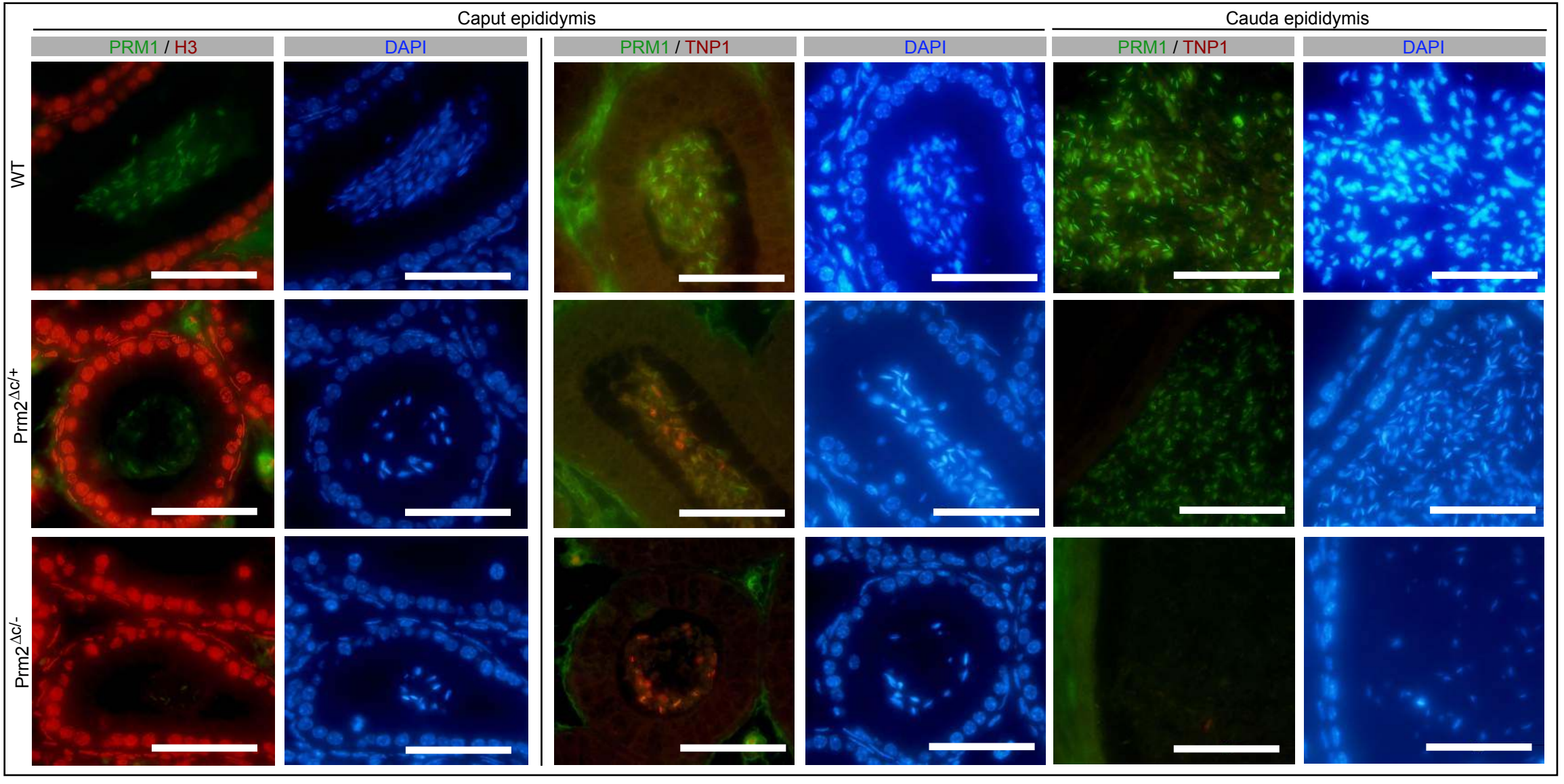

Fig. 5

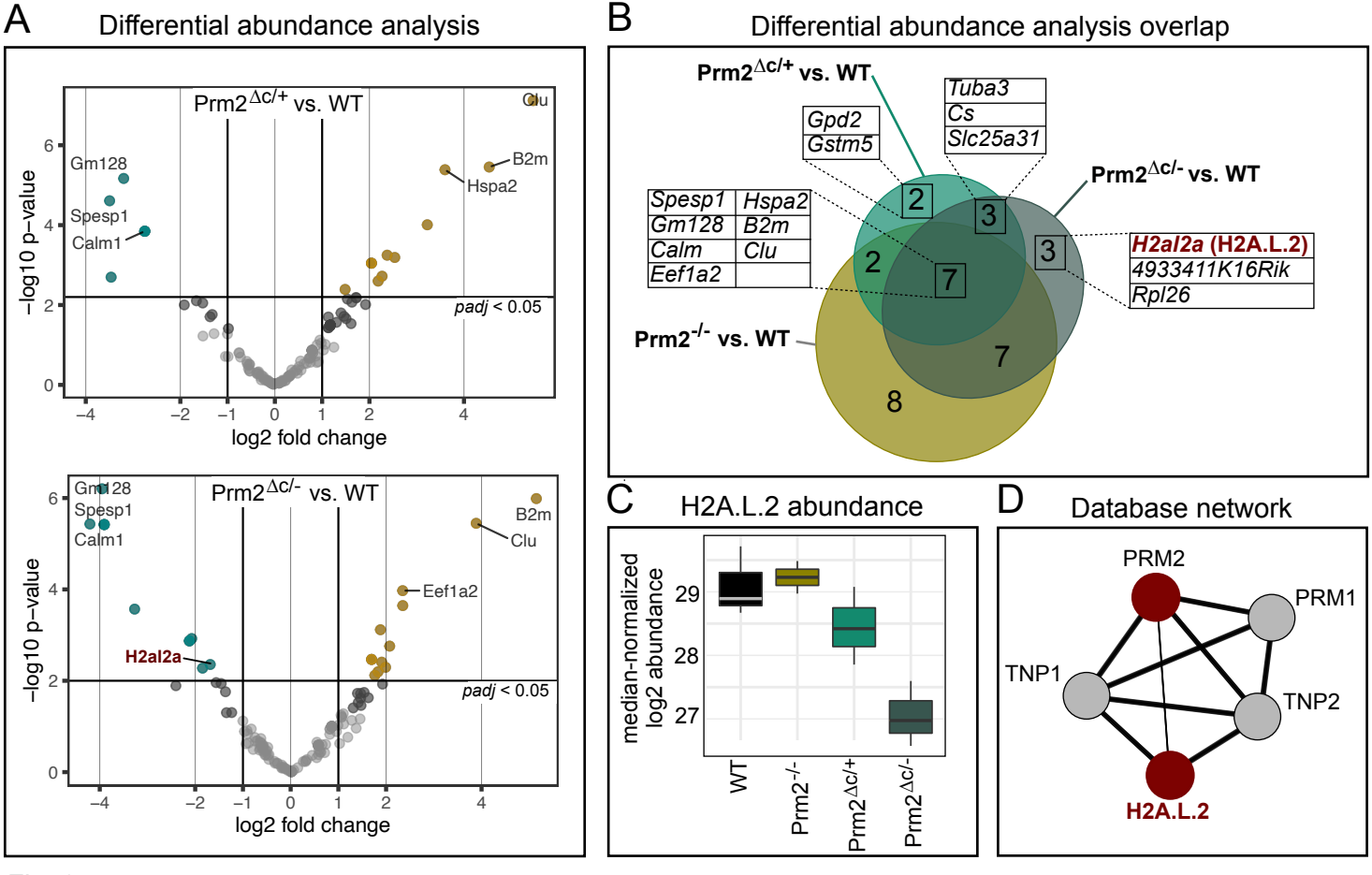
A
Differential abundance analysis
Prm2Δc/+ vs. WT
Clu
B2m
Hspa2
Gm128
Spesp1
Calm1
padj < 0.05
−log10 p−value
log2 fold change
Prm2Δc/- vs. WT
Gm128
Spesp1
Calm1
B2m
Clu
Eef1a2
H2al2a
padj < 0.05
−log10 p−value
log2 fold change
B
Differential abundance analysis overlap
Prm2Δc/+ vs. WT
Gpd2
Gstm5
Tuba3
Cs
Slc25a31
Prm2Δc/- vs. WT
Spesp1
Hspa2
Gm128
B2m
Calm
Clu
Eef1a2
H2al2a (H2A.L.2)
4933411K16Rik
Rpl26
Prm2-/- vs. WT
2
3
2
7
3
7
8
C
H2A.L.2 abundance
median-normalized log2 abundance
WT
Prm2-/-
Prm2Δc/+
Prm2Δc/-
D
Database network
PRM2
PRM1
TNP1
TNP2
H2A.L.2

Fig. 6

H2A.L.2 and PRM2 IHC

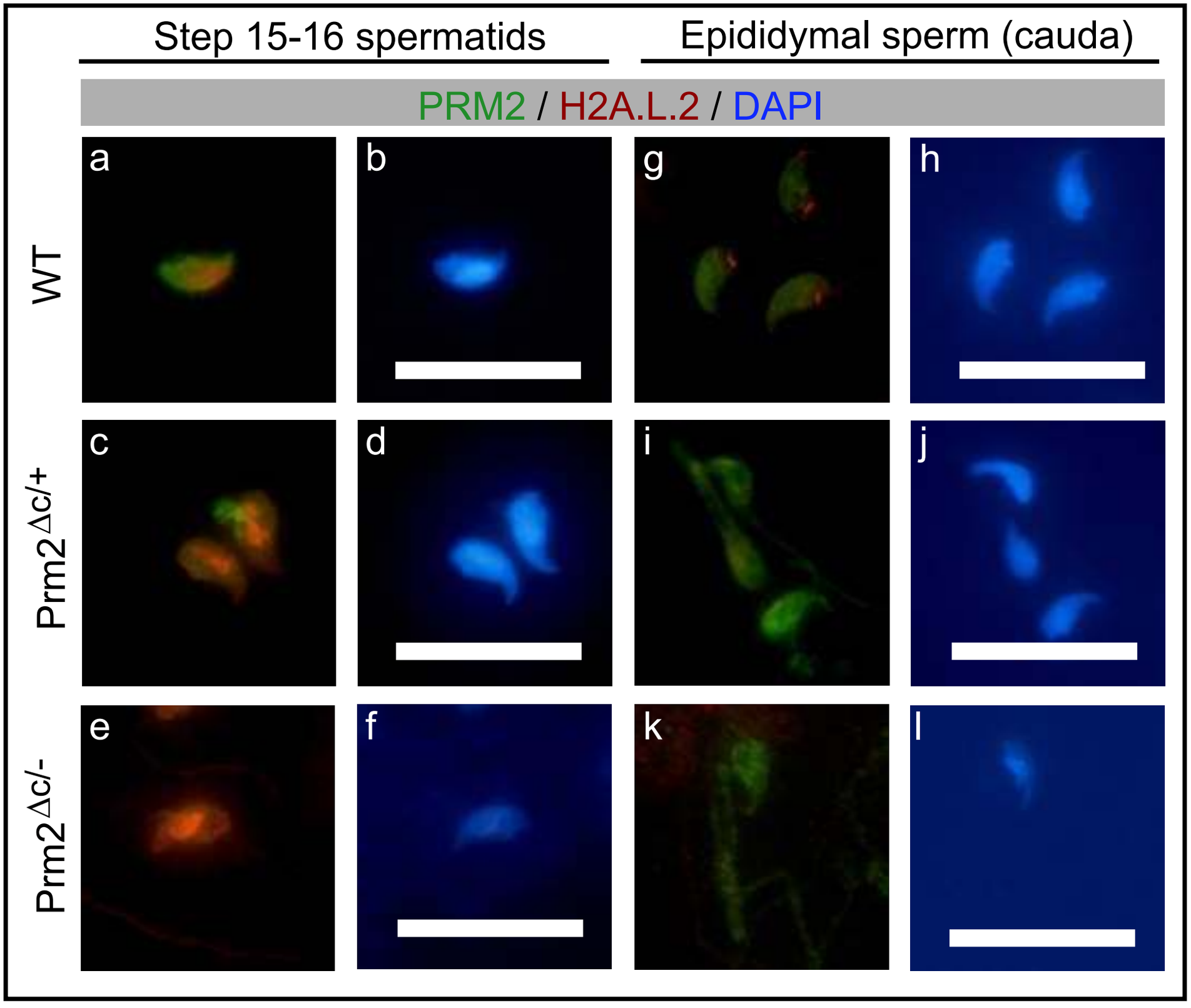

Fig. 7